Impacts of Stratospheric Sulfate Geoengineering on Tropospheric Ozone

(Supplemental Material)

Lili Xia[1*], Peer J. Nowack[2], Simone Tilmes[3] and Alan Robock[1]

[1]Department of Environmental Sciences, Rutgers University, New Brunswick, New Jersey, USA

[2]Centre for Atmospheric Science, Department of Chemistry, University of Cambridge, Cambridge, UK

[3]National Center of Atmospheric Research, Atmospheric Chemistry Division, Boulder, CO, USA

CESM1 (CAM-Chem) has been evaluated for the troposphere (Tilmes et al., 2016b) and has also been used for studies in the stratosphere (Fernandez et al., 2017). Here, we use the same model setup but for a higher horizontal resolution of 0.9° x 1.25° (called here the 1° version) instead of 1.9° x 2.5° (2° version), which is the version that is participating in the Chemistry Climate Model Initiative. Some differences in stratospheric column ozone between model versions occur (Fig. S1), likely due to slight differences in the stratospheric dynamics, for instance as result of differences in gravity waves. The 1° model shows some improvement in stratospheric column ozone in high northern latitudes in winter and spring as well as in summer in the high southern latitudes compared to the 2° version with regard to a present-day ozone climatology based on Ozone Monitoring Instrument (OMI) and Microwave Limb Sounder (MLS) satellite observations between 2004 and 2010, compiled by Ziemke et al. (2011). However, it also indicates an overestimation of the Antarctic ozone hole in October. Besides these differences, both versions reproduce observed column ozone very well.

Tropospheric ozone and other tracers (not shown) in both the 1° and the 2° model versions are very similar (Fig. S2) and are therefore not further discussed. A detailed description of the performance of the 2° simulation is given in Tilmes et al. (2016b).

Reference:

Tilmes, S., Lamarque, J.-F., Emmons, L. K., Conley, A., Schultz, M. G., Saunois, M., Thouret, V., Thompson, A. M., Oltmans, S. J., Johnson, B., and Tarasick, D.: Technical Note: Ozonesonde climatology between 1995 and 2011: description, evaluation and application, Atmos. Chem. Phys., 12, 7475-7497, doi:10.5194/acp-12-7475-2012, 2012.

Ziemke, J. R., Chandra, S., Labow, G. J., Bhartia, P. K., Froidevaux, L., and Witte, J. C.: A global climatology of tropospheric and stratospheric ozone derived from Aura OMI and MLS measurements, Atmos. Chem. Phys., 11, 9237-9251, doi:10.5194/acp-11-9237-2011, 2011.

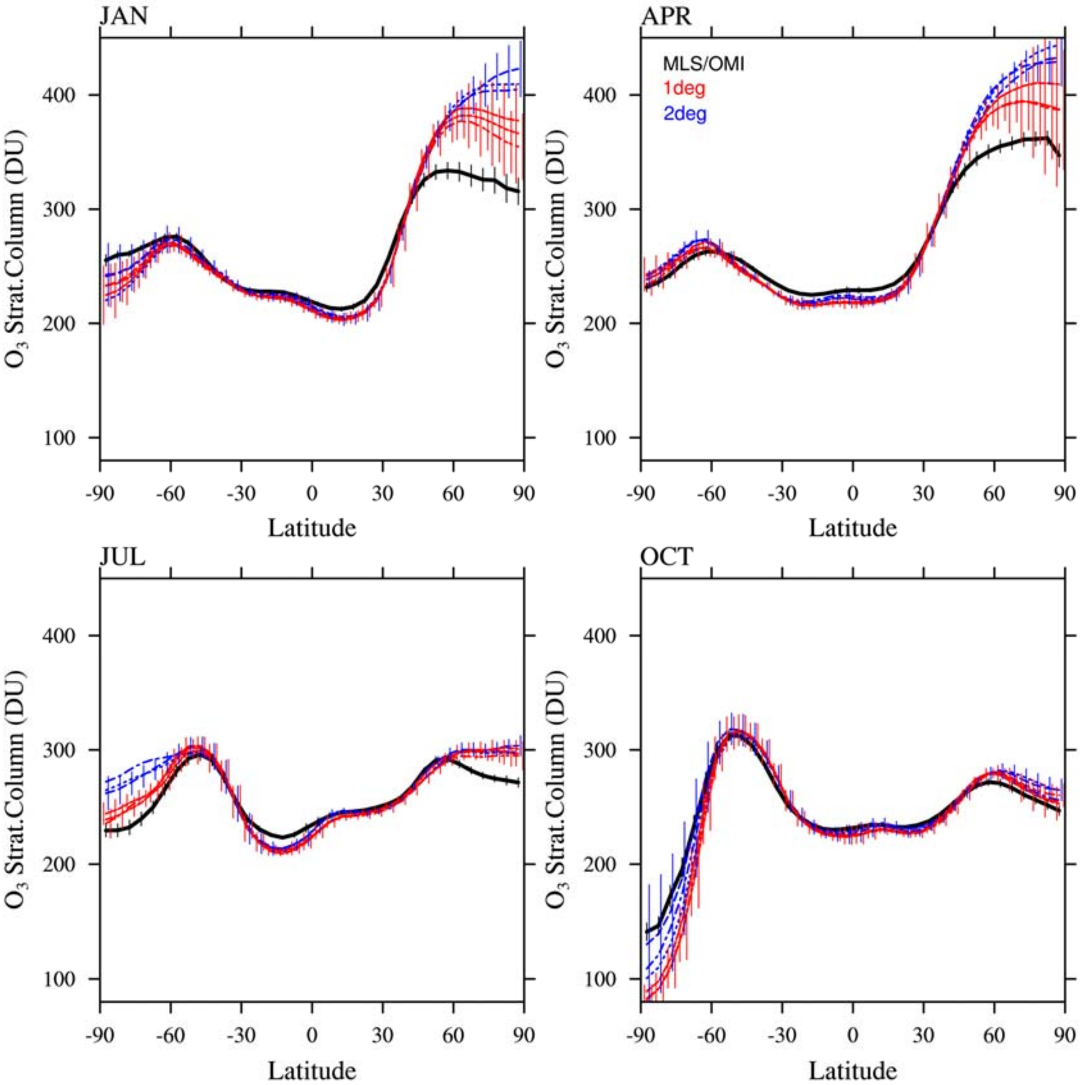

Figure S1. Monthly and zonally averaged stratospheric ozone column (in DU) comparison between the 10°N to 10°S gridded present day MLS/OMI satellite product (Ziemke et al., 2011) (black), CAM-Chem 1° simulation (red), and CAM-Chem 2° simulation (blue) for 2004-2010, shown for four months (different panels). The model tropopause to derive the stratospheric column is defined as the 150 ppb ozone level, while the climatological tropopause uses the World Meteorological Organization definition from the National Centers for Environmental Prediction. This may lead to small differences between observations and model simulations, but not between model experiments themselves. Model results are interpolated to the same grid as the observations and error bars indicate the ±1 standard deviation of the interannual variability for each latitude interval.

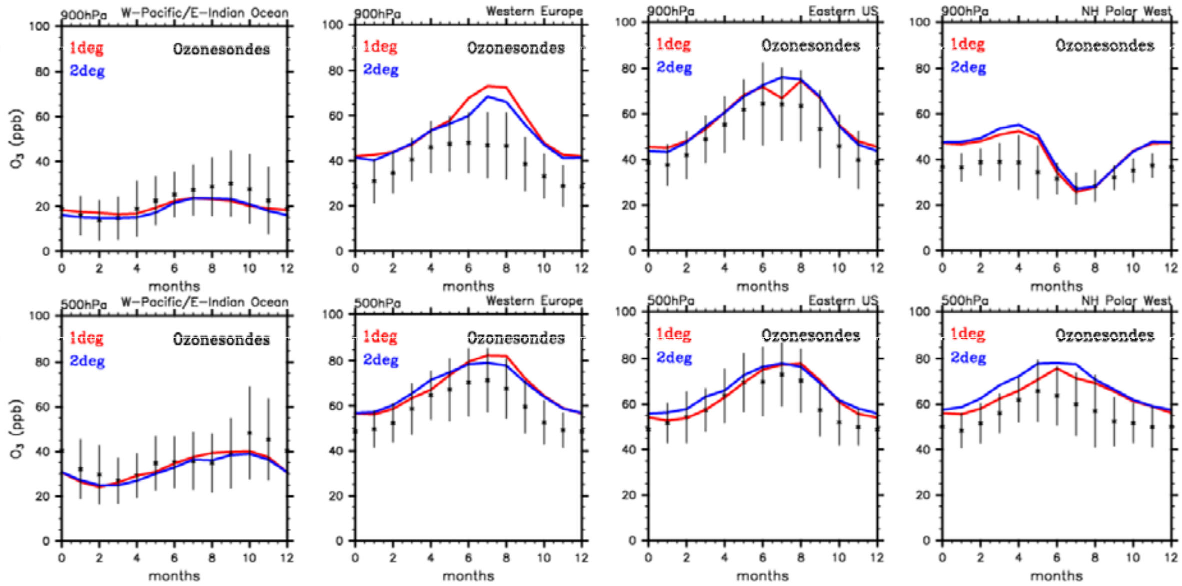

Figure S2. Regionally aggregated seasonal cycle comparisons of vertical measurements from ozone soundings (in ppb) averaged between 1995 and 2010 (black lines) (Tilmes et al., 2012), and CAM-Chem 1° results (red), and CAM-Chem 2° results (blue) averaged between 2005 and 2010, interpolated to 900 mb (top) and 500 mb (bottom).

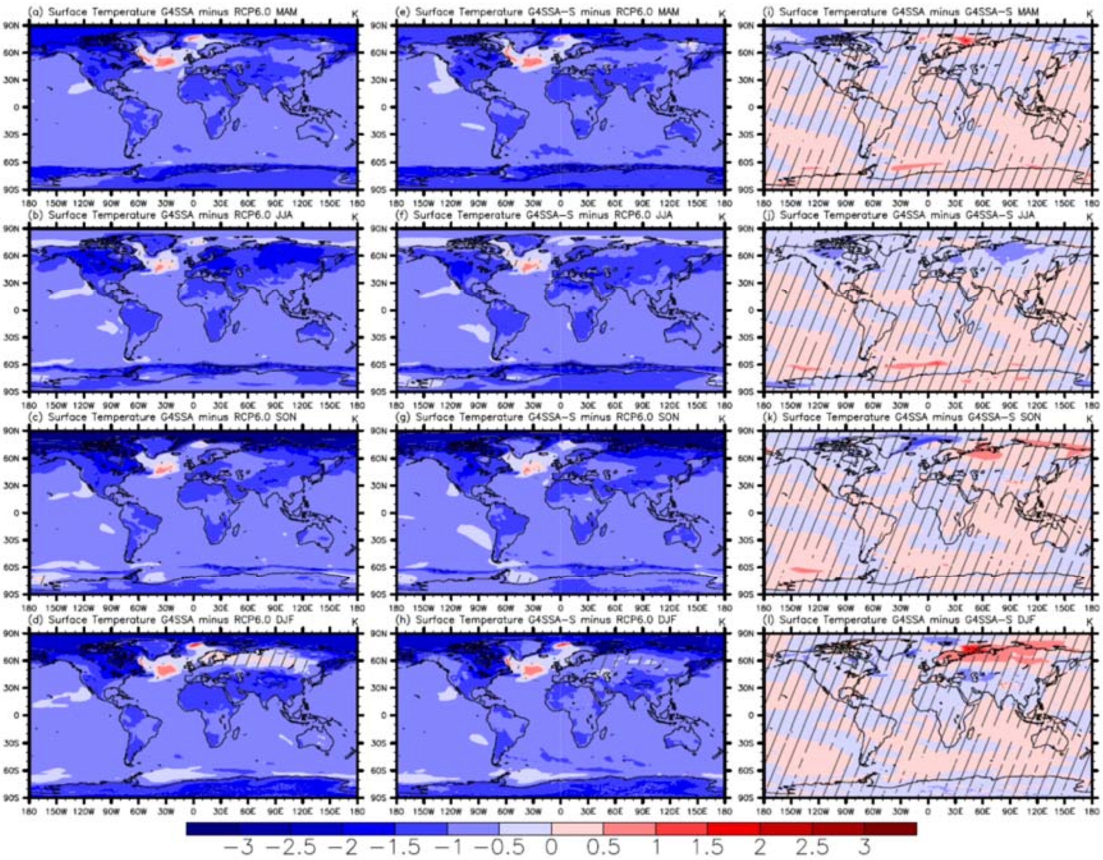

Figure S3. Global map of seasonal surface temperature differences (K) between G4SSA and RCP6.0 (left column), G4SSA-S and RCP6.0 (middle column) and G4SSA and G4SSA-S (right column) for 2030-2069. Hatched regions are areas with $p > 0.05$ (where changes are not statistically significant based on a paired *t*-test).

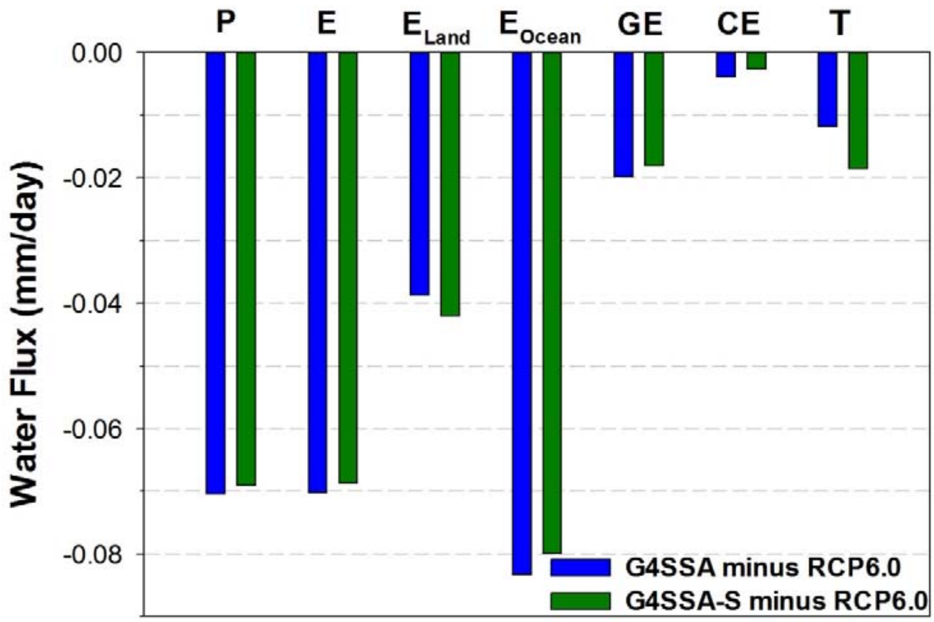

Figure S4. Surface water flux differences, shown as G4SSA minus RCP6.0 and G4SSA-S minus RCP6.0 for 2030-2069. P is precipitation. E is total evaporation. GE is ground evaporation, which is the sum of soil evaporation, snow evaporation, soil sublimation, and snow sublimation minus dew. CE is canopy evaporation and T is transpiration. For P, positive is downward, and for all the other fluxes, positive is upward.

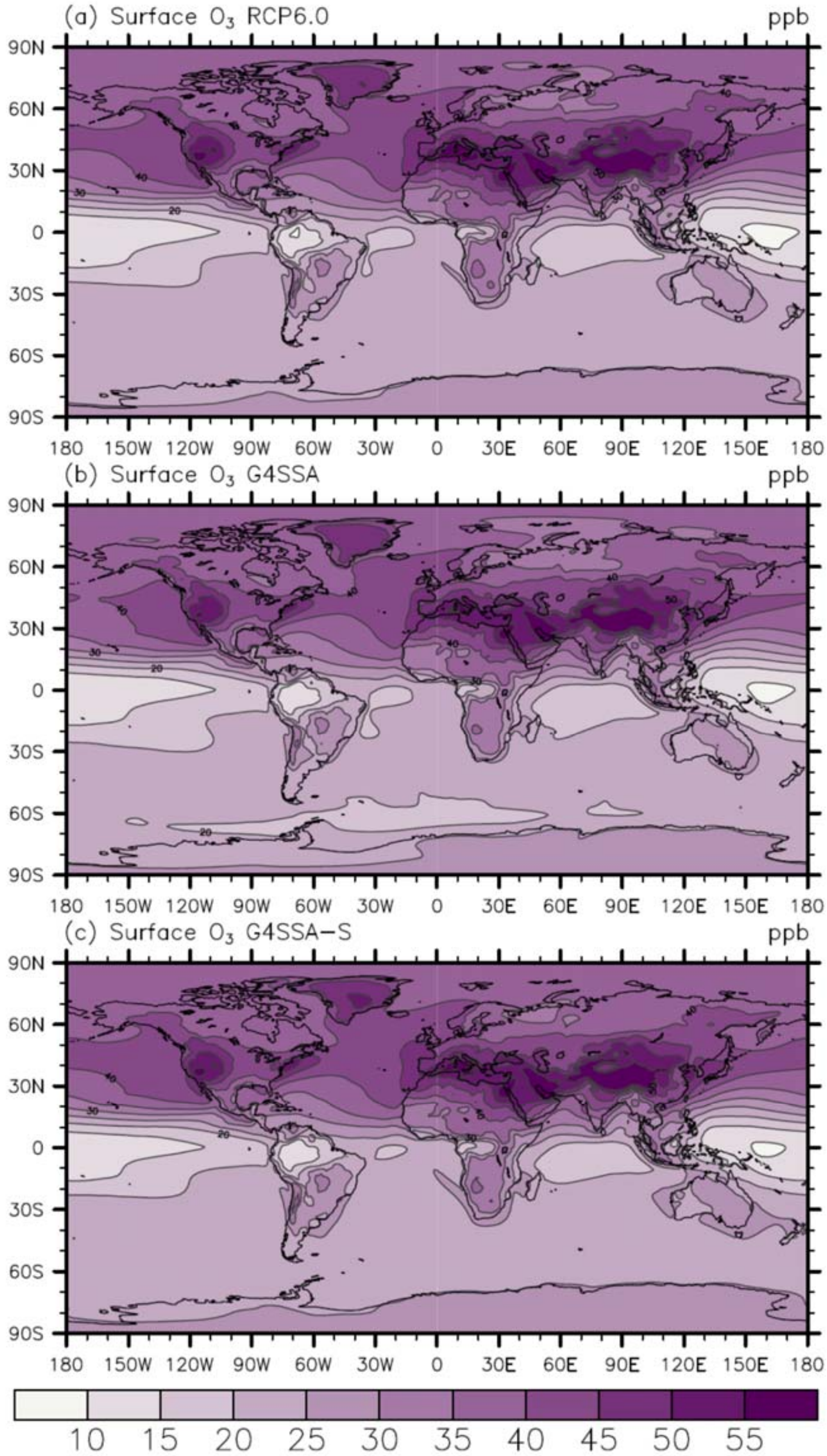

Figure S5. Global map of surface ozone concentration (ppb) in (a) RCP6.0, (b) G4SSA and (c) G4SSA-S for 2030-2069.

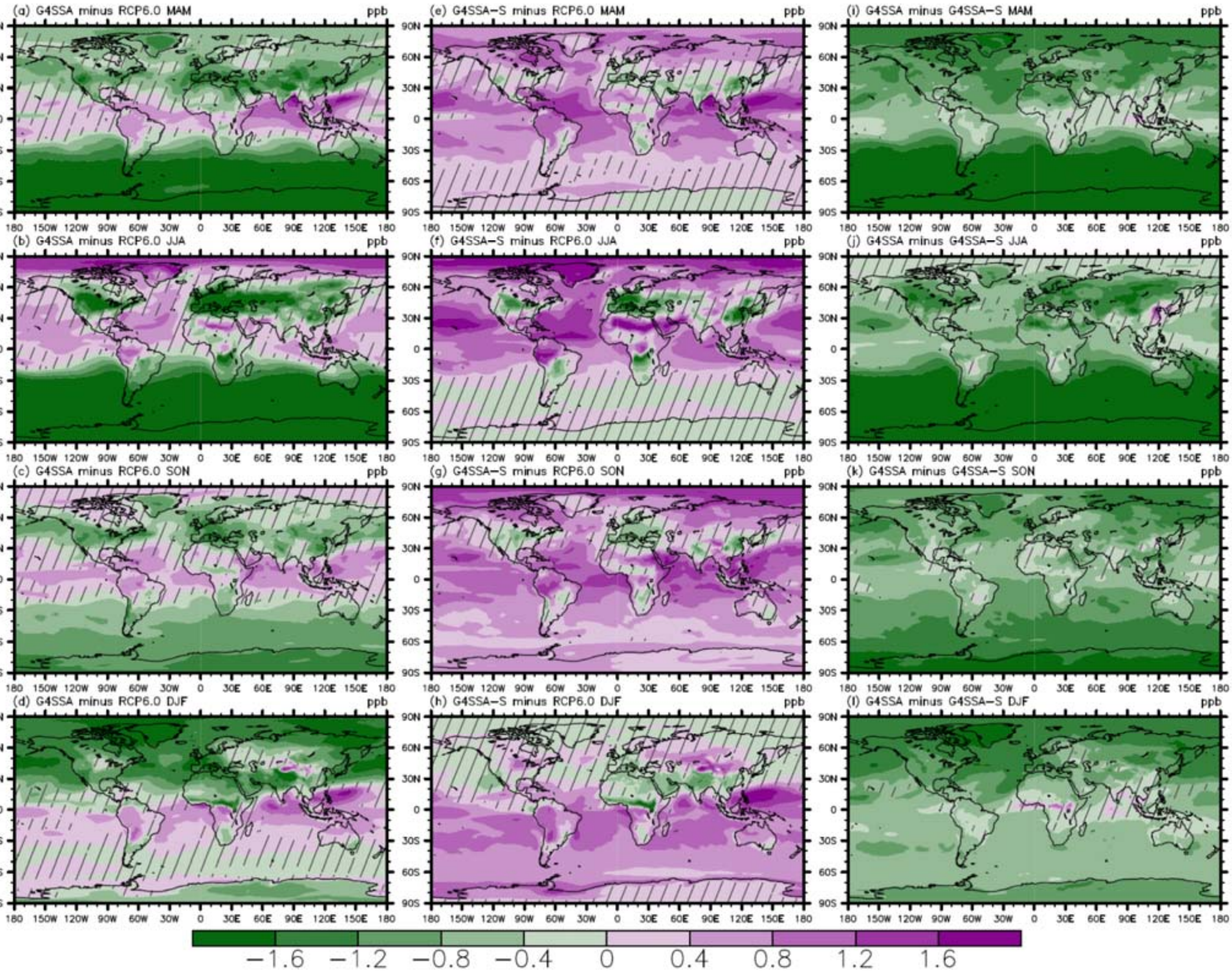

Figure S6. Global map of seasonal surface ozone concentration differences (ppb) between G4SSA and RCP6.0 (left column), G4SSA-S and RCP6.0 (middle column) and G4SSA and G4SSA-S (right column) for 2030-2069. Hatched regions are areas with $p > 0.05$.

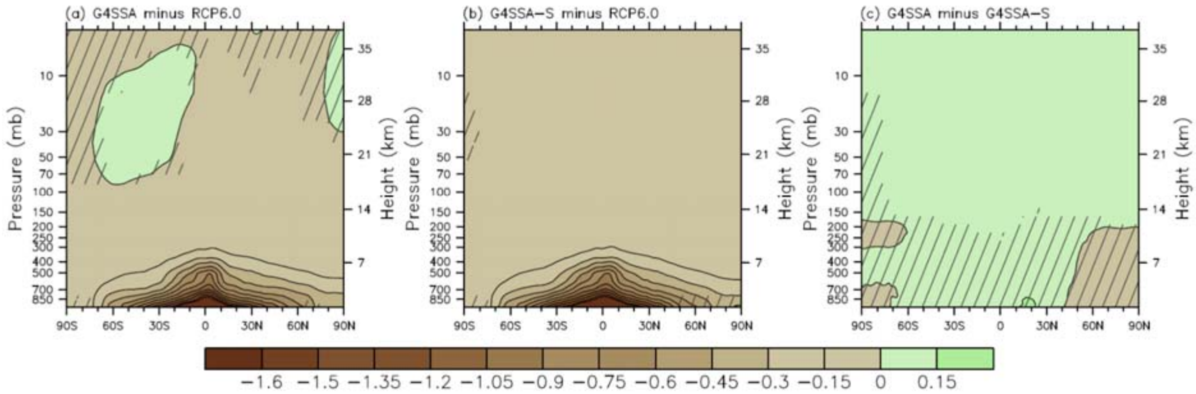

Figure S7. Zonal mean water vapor mixing ratio differences (g kg^{-1}) in the geoengineering experiments (a) G4SSA minus RCP6.0, (b) G4SSA-S minus RCP6.0, and (c) G4SSA minus G4SSA-S. These are averaged for three ensemble members for years 2030-2069. Hatched regions are areas with $p > 0.05$.

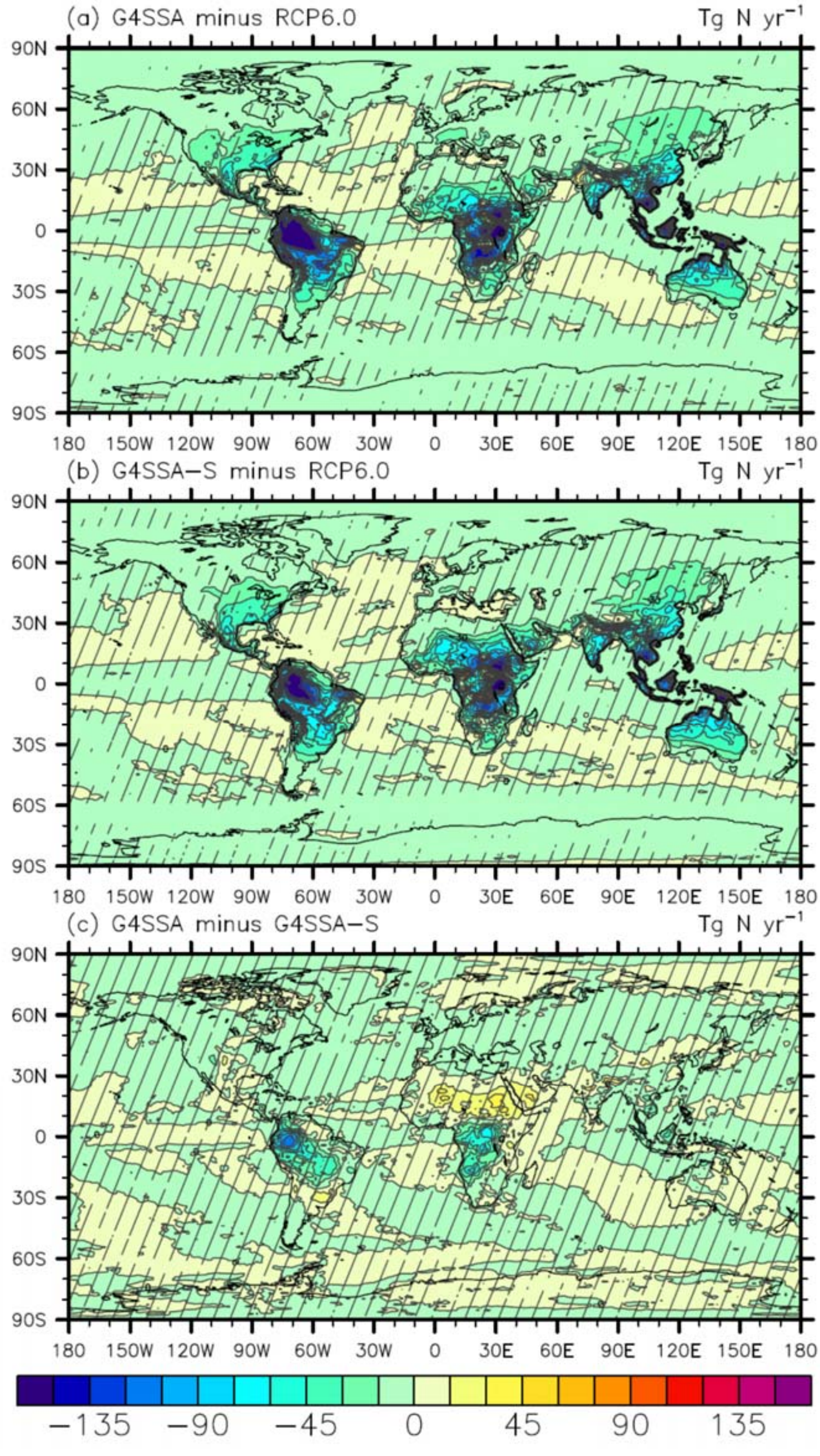

Figure S8. Global map of differences of column NO produced by lightning (Tg N yr^{-1}) between (a), G4SSA and RCP6.0, (b) G4SSA-S and RCP6.0, and (c) G4SSA and G4SSA-S for 2030-2069. Hatched regions are areas with $p > 0.05$.

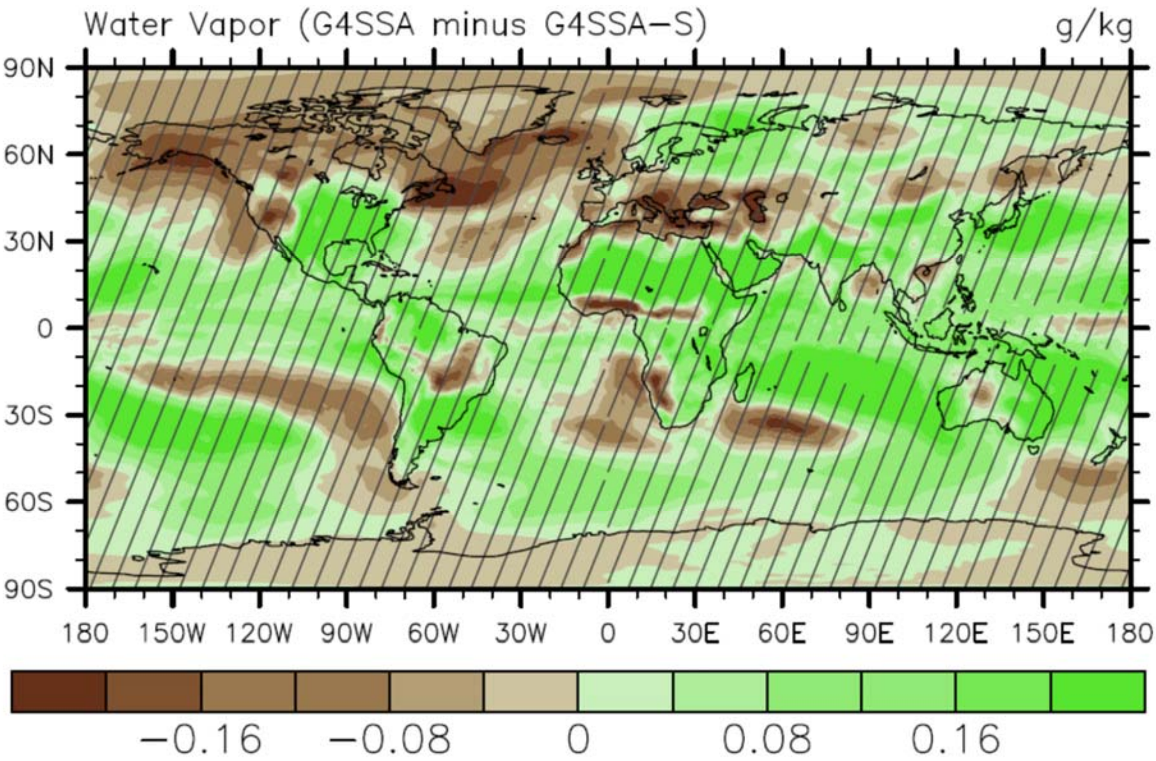

Figure S9. Global map of surface water vapor mixing ratio difference (g kg^{-1}) between G4SSA and G4SSA-S over the period of years 2030-2069. Hatched regions are areas with $p > 0.05$.

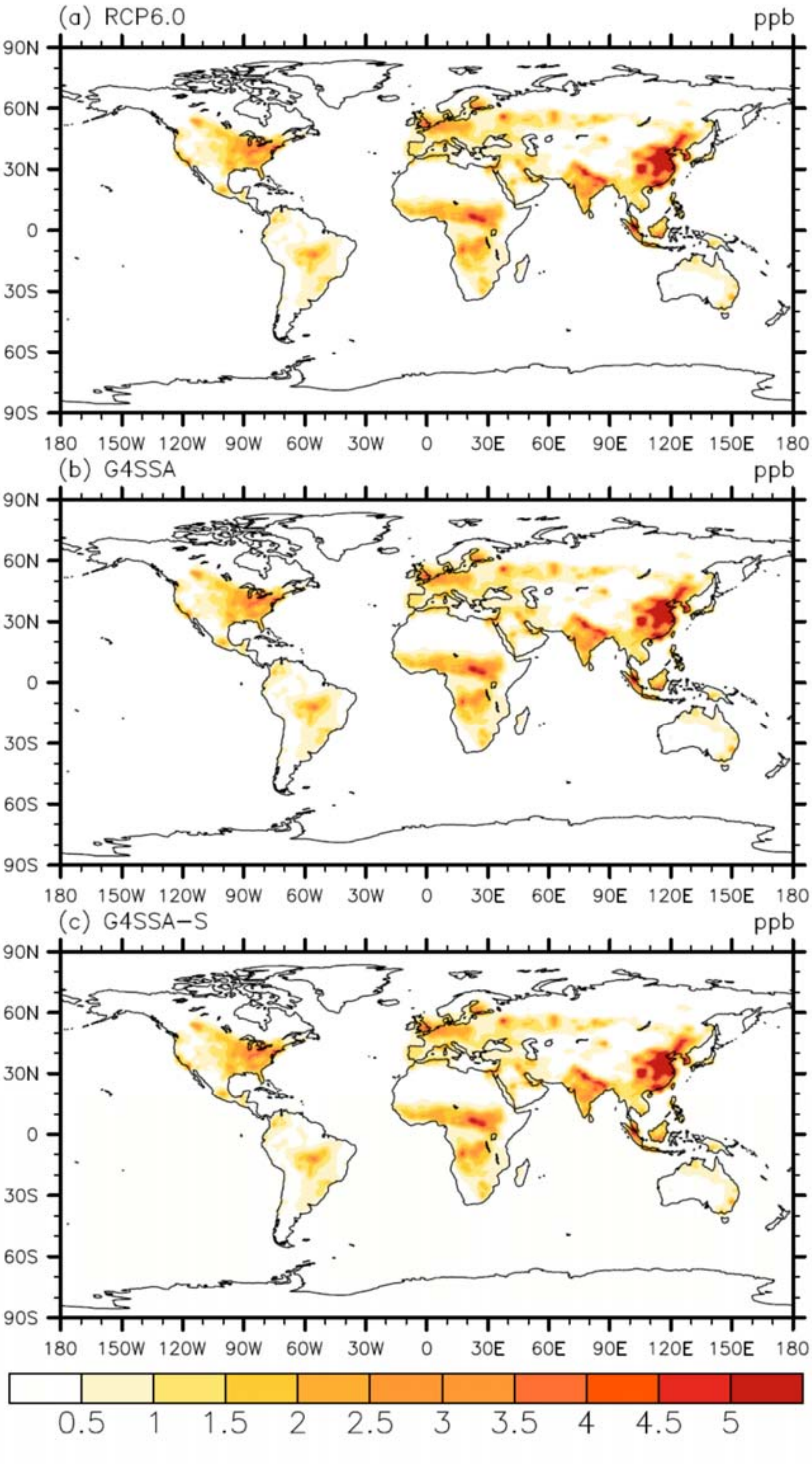

Figure S10. Global map of surface NO_x concentration (ppb) in (a) RCP6.0, (b) G4SSA and (c) G4SSA-S for 2030-2069.

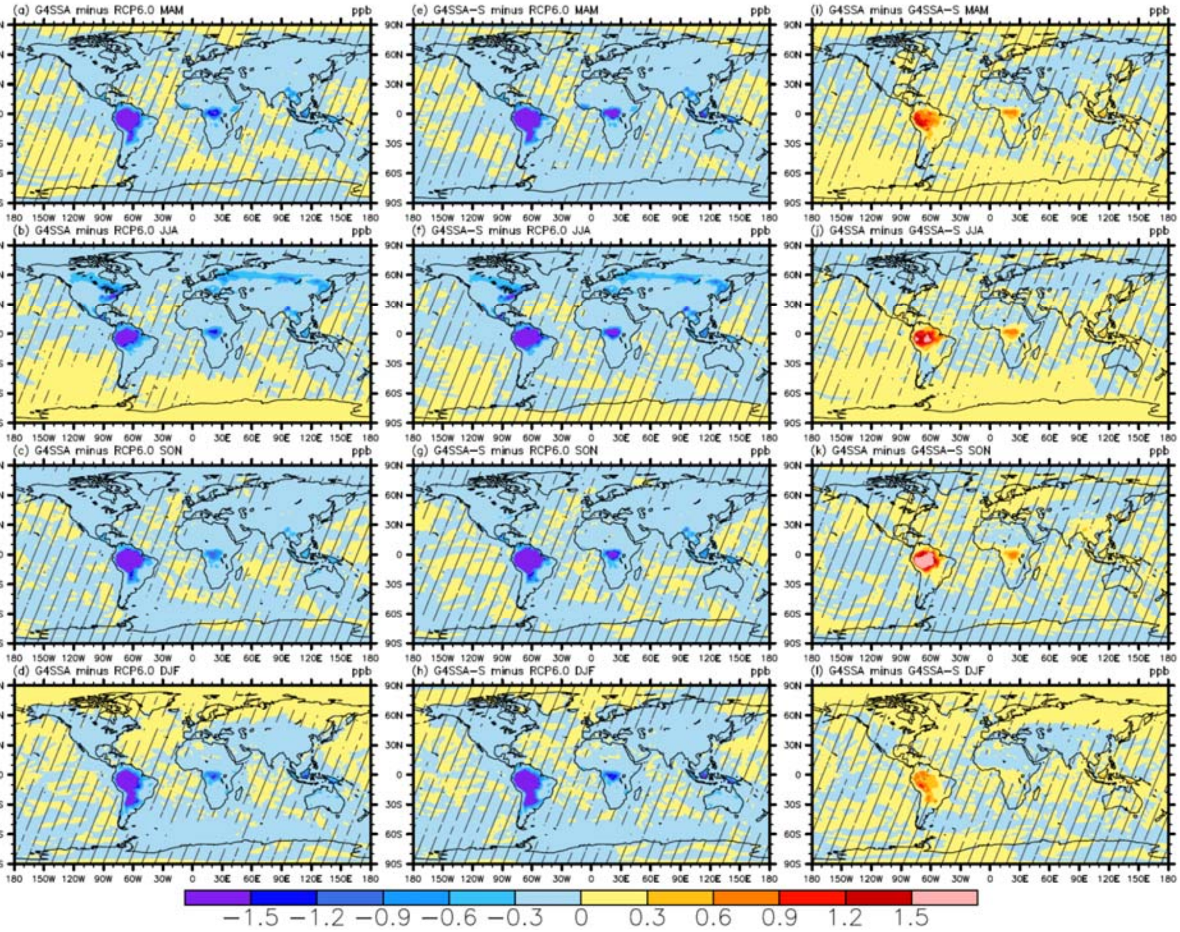

Figure S11. Global map of seasonal surface bio-emitted isoprene concentration differences (ppb) between G4SSA and RCP6.0 (left column), G4SSA-S and RCP6.0 (middle column) and G4SSA and G4SSA-S (right column) for 2030-2069. Hatched regions are areas with $p > 0.05$.

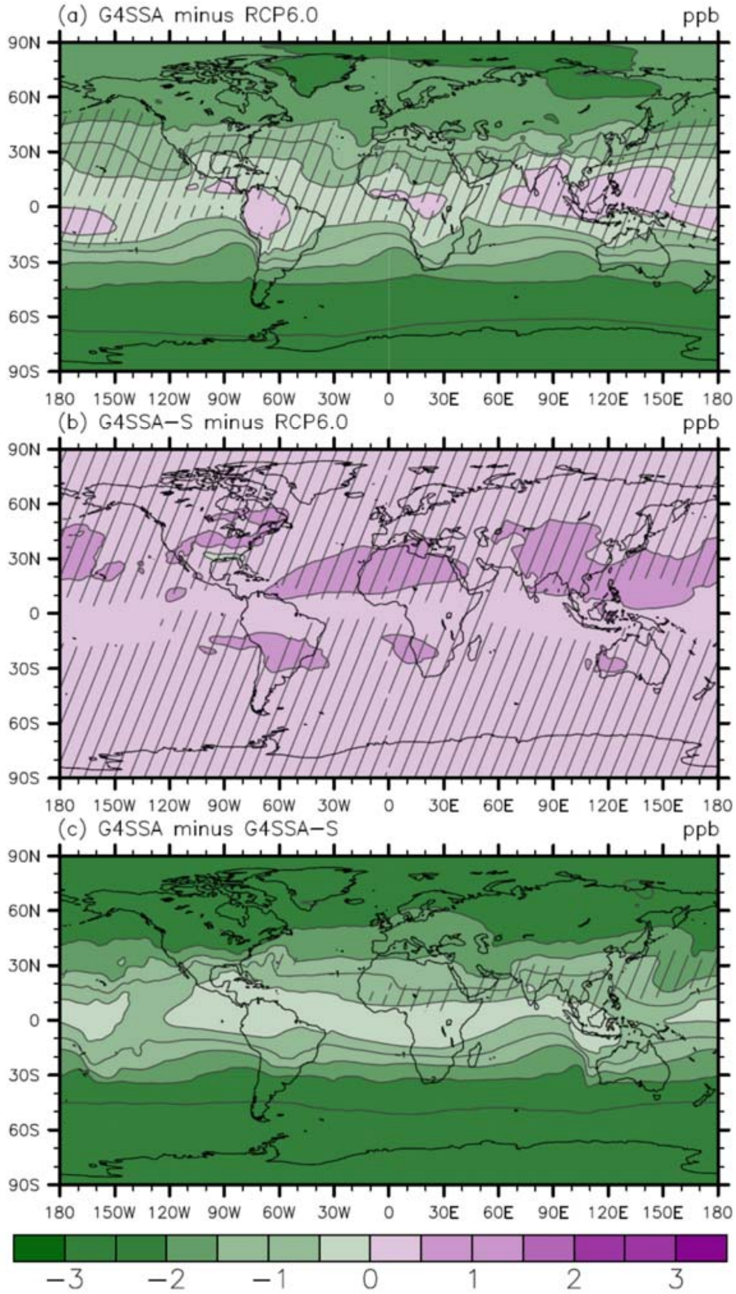

Figure S12. Global map of surface O_3^{Strat} differences (ppb) between (a), G4SSA and RCP6.0, (b) G4SSA-S and RCP6.0, and (c) G4SSA and G4SSA-S for 2030-2069. Hatched regions are areas with $p > 0.05$. There is much less O_3^{Strat} at the surface in G4SSA relative to RCP6.0 as well as G4SSA-S. Changes in O_3^{Strat} at the surface are on the one hand due to reduced ozone in the stratosphere, and on the other hand due to to changes in the rate of STE. Although the absolute value of O_3^{Strat} is overestimated, because of a missing loss process via dry depostion in the version of the model, it can be qualitatively used to compare the two scenarios, since dry deposion is not expected to change significantly.